A probabilistic risk assessment framework considering lane-changing behavior interaction

Heye HUANG[1], Jianqiang WANG[1], Cong FEI[1], Xunjia ZHENG[1*], Yibin YANG[1],
Jinxin LIU[1], Xiangbin WU[2] & Qing XU[1*]

[1]*The State Key Laboratory of Automotive Safety and Energy, Tsinghua University, Beijing* 100084, *China;*
[2]*Intel, Beijing* 100084, *China*

Abstract   Understanding the dynamic characteristics of surrounding vehicles and estimating the potential risk of mixed traffic can help reliable autonomous driving. However, the existing risk assessment methods are challenging to detect dangerous situations in advance and tackle the uncertainty of mixed traffic. In this paper, we propose a probabilistic driving risk assessment framework based on intention identification and risk assessment of surrounding vehicles. Firstly, we set up an intention identification model (IIM) via long short-term memory (LSTM) networks to identify the intention possibility of the surrounding vehicles. Then a risk assessment model (RAM) based on the driving safety field is employed to output the potential risk. Specifically, driving safety field can reflect the coupling relationship of drivers, vehicles, and roads by analyzing their interaction. Finally, an integrated risk evaluation model combining both IIM and RAM is developed to form a dynamic potential risk map considering multi-vehicle interaction. For example, in a typical but challenging lane-changing scenario, an intelligent vehicle can assess its driving status by calculating a risk map in real time that represents the risk generated by the estimated intentions of surrounding vehicles. Furthermore, simulations and naturalistic driving experiments are conducted in the extracted lane-changing scenarios, and the results verify the effectiveness of the proposed model considering lane-changing behavior interaction.

Keywords   behavior probability, risk assessment, intention identification, LSTM, driving safety field

1   Introduction

The development of automated driving technology brings convenience to people's travel and transportation, and makes safety and reliable autonomous driving a research hotspot [1–3]. Intelligent vehicles are supposed to assess current environmental risks for ensuring safe and efficient autonomous driving [4], while the uncertainty and dynamic changes in the traffic environment make it challenging to carry out reliable risk assessment. Key problems exist in how to quantitatively assess driving risk in dynamic mixed traffic environment considering the multi-vehicle interaction. Therefore, by assessing driving risks and accurately identifying risk trends, the automated driving system can achieve obstacle avoidance more effectively and truly realize vehicle trajectory planning and tracking [5]. A feasible solution to improving the accuracy is to further introduce intention identification of traffic participants based on the existing determined risk assessment methods [4, 6].

---

* Corresponding author (email: zhengxj15@mails.tsinghua.edu.cn, qingxu@tsinghua.edu.cn)

Risk assessment has obtained extensive research owing to the application requirements [7,8]. From the perspective of introducing prior information of multi-vehicle interaction, modeling risk assessment can be classified into two main categories: deterministic risk assessment methods and uncertainty-based risk assessment methods. Deterministic risk assessment methods usually take little account of the intentions of surrounding vehicles and limit in coping with the uncertainty of mixed traffic. They can be roughly classified into distance-based logic methods, time-based logic methods and potential field methods. The distance logic method employs the safety distance in space as the risk evaluation index, and typical representatives include MAZDA model, HONDA model, NHSTA model [9,10], fixed distance model [9], and kinematics model [11]. The time logic method uses the safe distance in time as the risk evaluation index, such as the time to collision (TTC) [12], TTCA [13], and time headway (THW) [14]. Most of these methods are based on vehicle kinematics and dynamics theory. Furthermore, the description of driving risk is mostly based on vehicle state/relative motion information. These methods are useful because of their simple parameters and their physical meaning conforms to individuals' subjective feelings. However, these methods are usually limited to one-dimensional (longitudinal or lateral) risk assessment, which is difficult to realize high dimensional uncertainty risk assessment in real traffic, and suffers the limited practical application.

Since Khatib [15] first proposed the artificial potential field (APF) method, the research on describing the driving risk by employing potential field has been continuously developed. Reichardt et al. [16] proposed an electric field model based on APF to describe the risk distribution of vehicles in traffic environment, thus guiding the safe decision-making. Cao et al. [17,18] applied the APF method to avoid collision between ego vehicle and other obstacles by establishing an integrated model combining road/vehicle/speed potential field. These APF methods can realize high dimensional risk assessment, achieve better risk-sensitive and accuracy in complex traffic. However, they rarely consider the impact of uncertain factors such as the driver characteristics, vehicle dynamics, road condition and weather. Wang et al. [19] put forward a unified model of using the concept of driving safety field that considered the comprehensive factors of drivers, vehicles, and roads. The unified model can quantify the driving risks by systematically modeling the coupling relationship of traffic system, but limit in evaluating the traffic elements in the current environment without dynamic consideration of potential risk trends. Further, the above deterministic methods are usually taken as sub-optimal or limited in accuracy for little considering environment-vehicle interaction.

Another kind of risk assessment methods considering the prior intention can take more account of environmental uncertainty and interaction of behaviors. The uncertainty-based risk assessment method, also called as the intention-based risk assessment method, generally has two main steps. First, it will estimate the intention of driving behaviors, and then output the collision probability of the future trajectory to calculate the risk degree. These methods usually identify the intention driven by model or data and mainly include support vector machine (SVM) [20], Hidden Markov model (HMM) [21], Bayesian formulation [22], the Monte Carlo simulation (MC) [23] and Kalman Filter (KF). Xie et al. [22] combined the physics- and maneuver-based prediction model via a Bayesian network to make situational assessment, and achieved a high accuracy in lane-changing scenarios. Aoude et al. [20] employed an intention predictor based on SVM and rapidly-exploring random trees to estimate risk at intersection. Ref. [24] combined KF and Gaussian distribution to predict the future trajectory distribution and then computed the collision probability, which can achieve good performance in simulation scenes. Meanwhile, long short-term memory (LSTM) has made a series of breakthroughs in speech recognition, machine translation, image captioning, etc., owing to its depth representation ability in time series problem processing. Therefore, a number of research applied LSTM to predict trajectories, and achieved better prediction results [25,26]. However, although these methods can give more consideration to input the intention for identification, they consider finite factors such as road geometry or driver characteristics. Further, these methods simplify the physical models and limit in describing the coupling mechanism of drivers, vehicles and roads clearly, which constrains their application in specific scenarios and has difficulty to be widely employed in mixed traffic.

Therefore, in this paper, we develop an intention-based risk assessment algorithm, as shown in Fig-
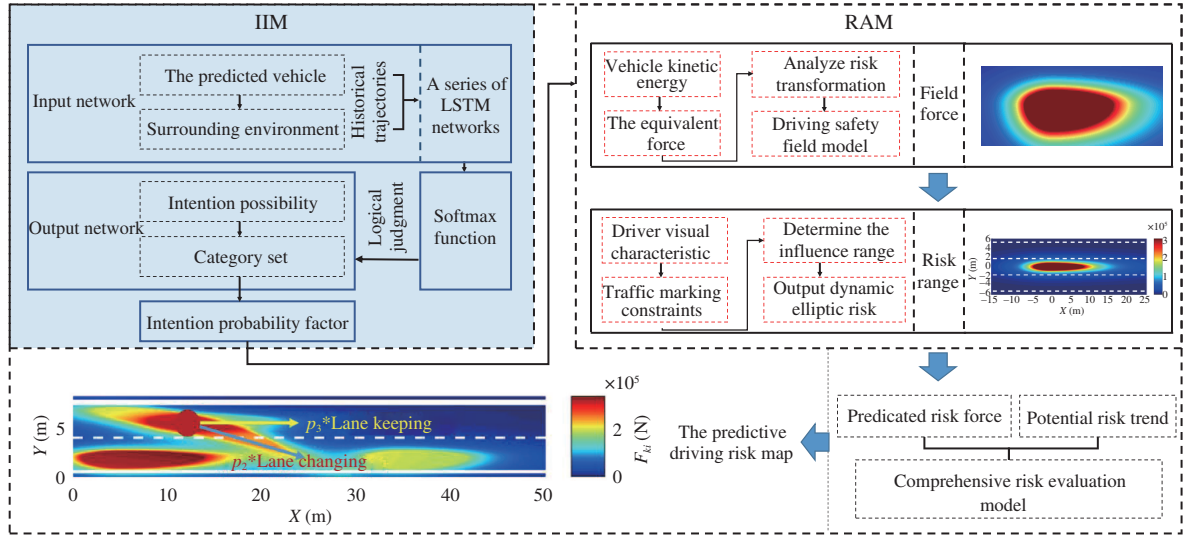
Figure 1 (Color online) The framework of the comprehensive risk evaluation model. The combined model is composed of an intention identification model (IIM) and a risk assessment model (RAM). The IIM outputs the intention possibilities to the RAM. The RAM describes the dynamic magnitude and influence range of driving risk. Finally, a predictive risk map is generated to quantify the potential risk.

ure 1. We first develop an intention identification model (IIM) by employing the LSTM networks to identify the intention of traffic participants in surrounding environment, and then propose a high dimensional advanced driving safety field defining the interaction with multi-vehicles and risk influence range. To the end, by inputting the intention probability factor to the risk assessment model (RAM), an integrated model is developed to accurately evaluate the driving risk in dynamic traffic environment. Main contributions can be included in three aspects. First, we tackle the risk estimation problem from a new perspective: an integrated framework is developed by inferring intention probability and potential risk from hierarchic analysis, while distinguished from traditional methods typically from overall aspect. Then, considering the problems of the existing risk identification models, we focus on analyzing the factors that affect driving safety and the potential influence scope of driving risks, and present a high dimensional and time-varying RAM. Finally, with the consideration of risk trends and traffic participants' interaction, the proposed method can improve the accuracy of driving risk identification and provide pre-warning compared with other existing methods.

2 Intention identification of traffic participants

The ability to predict the movement trends of surrounding vehicles can allow intelligent vehicles to assess driving risk in dynamic scenes more accurately. Besides, the input of prior information can avoid dangerous scenes, and make reasonable decision planning for automated vehicles in advance. Based on LSTM networks, the IIM regards the predicted vehicles and their surrounding vehicles as a whole, and then it can understand the interactive behavior between multi-vehicles and dynamically identify the vehicles' intentions.

2.1 The framework of IIM

The IIM proposed in this paper is supposed to understand the traffic rules according to vehicle-environment interaction information and predict the driving intention of surrounding vehicles. The structural framework is shown in Figure 2. The whole model is built based on a series of LSTM networks. The Softmax layer outputs the identification vector of driving intention and sets the appropriate threshold to avoid the model from making the conservative predictions all the time. The input module uses two LSTM networks to construct an encoder and a decoder respectively. The encoder and decoder work collaboratively in the
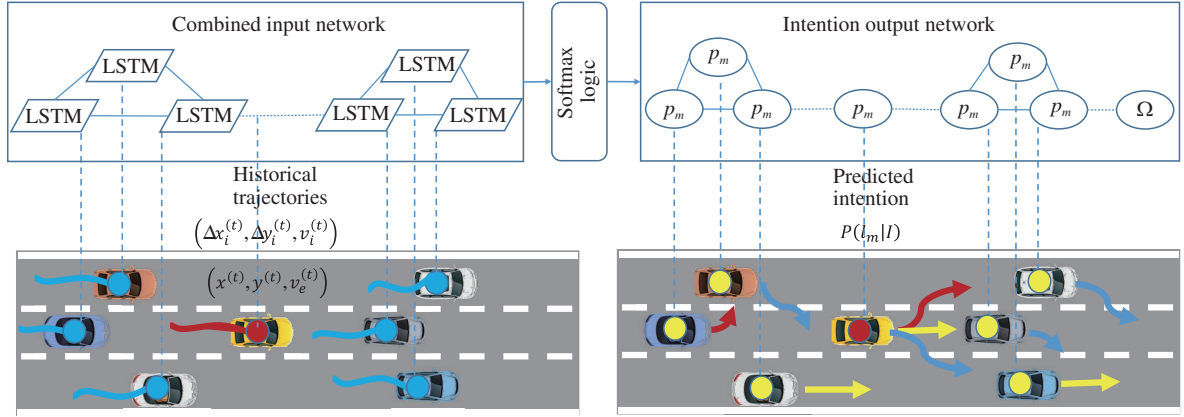
Figure 2 (Color online) The structure of IIM. The input network includes a series of LSTM networks, and the output network generates the intention probabilities.

input network, in which historical trajectories are fed into the encoder, and then the encoding vectors consisting of driving intention information are input to the decoder. Finally, the decoder can predict the intention probability. The basic steps of constructing an IIM can summarized as follows. (1) Input the historical trajectory information I (speed and position) of surrounding vehicles and the predicted vehicle into the LSTM network. (2) Employ the activation function of Softmax, and define the logical judgment on the basis of probability maximum classification; specifically, to increase the accuracy of intention identification, we set a logical judgment on the output probability, and specify that the confidence threshold of left and right lane changes is 80% and that of straight line driving is 70%. When the hypothetical intention of a certain type is greater than the corresponding certainty threshold, it is determined to be the correct type, so the probability of this type is adjusted to 1, and the probabilities of the other two types are 0. (3) Output the probabilities p_m $(m = 1, 2, 3)$ of different driving intentions for each category in the intent category vector $L = (l_1, l_2, l_3)$. Specifically,

$$p_m = P\left(l_m | I\right), \quad \Omega = (p_1, p_2, p_3), \tag{1}$$

where p_m is defined as the intention identification factor. The sum of p_m $(m = 1, 2, 3)$ is equal to 1.

Considering the interactive information, we regard the surrounding vehicles in the real traffic scene as an interdependent entirety, and their manipulation behaviors affect each other's decisions. To understand the vehicle-environment interaction better, we express the detailed input information including the historical trajectory information and environmental information of the predicted vehicle as

$$I^{(t)} = \left[V_e^{(t)}, S^{(t)}\right], \quad t = (T - T_p, \ldots, T - 1, T), \tag{2}$$

where $V_e^{(t)}$ is the historical information of the predicted vehicle; $S^{(t)}$ is surrounding environmental information; T_p is a historical time-domain (reflecting the length of the input trajectory). Referring to the lane change time in highway environment being generally between 3.5 s and 6 s, an average time of 5 s can realize a complete lane change process [27]. Therefore, we define $T_p = 3$ s to determine the length of historical trajectories.

Specifically, the state information of the predicted vehicle includes $V_e^{(t)} = (x^{(t)}, y^{(t)}, v_e^{(t)})$, where $x^{(t)}$ is the lateral coordinates of the predicted vehicle, $y^{(t)}$ is the longitudinal coordinates of the predicted vehicle, and $v_e^{(t)}$ is the absolute velocity of the predicted vehicle.

The environmental information, denoted by $S^{(t)}$, consists of the historical trajectory information of the surrounding vehicles and two flag bits of the predicted vehicle. Specific surrounding direction includes the left front, the right front, the straight ahead, the left rear, the right rear, and the straight back (denoted by ID 1, 2, 3, 4, 5, 6, respectively, and the positional relationship is shown in Figure 3). The environmental information $S^{(t)}$ is represented as follows:
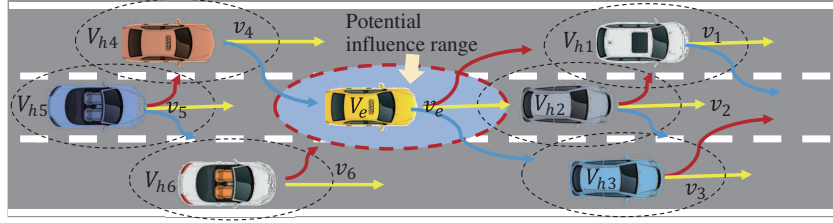
Figure 3 (Color online) Schematic diagram of the predicted vehicle and its surrounding environment. The predicted vehicle v_e is surrounded by six other vehicles ($V_{h1} - V_{h6}$), and the potential intentions of these vehicles are described by the lines with different colors. Each vehicle has its potential influence range shown as an ellipse in the figure.

$$S^{(t)} = \left(V_{h1}^{(t)}, V_{h2}^{(t)}, V_{h3}^{(t)}, V_{h4}^{(t)}, V_{h5}^{(t)}, V_{h6}^{(t)}, C_r^{(t)}, C_l^{(t)} \right). \tag{3}$$

Particularly, the status information of surrounding vehicles includes their positions and speeds:

$$V_{hi}^{(t)} = \left(\Delta x_i^{(t)}, \Delta y_i^{(t)}, v_i^{(t)} \right), \tag{4}$$

where $\Delta x_i^{(t)}$ is the lateral relative distance between the ith location vehicle and the predicted vehicle; $\Delta y_i^{(t)}$ is the longitudinal relative distance between the ith location vehicle and the predicted vehicle; $v_i^{(t)}$ represents the absolute speed of the ith location vehicle; $C_r^{(t)}$ is the right lane flag (if there is a right lane of the predicted vehicle, marked as 1; otherwise 0); $C_l^{(t)}$ is the left lane flag (if there is a right lane of the predicted vehicle, marked as 1; otherwise 0).

To avoid over-fitting, we set the number of hidden cells in LSTM network as 128, and construct the deep circulation neural network structure by stacking 4 circulation layers. The dropout ratio between circulation bodies in different layers is 0.2. Because the IIM is a classifier, the data preprocessing step needs to attach the corresponding category set C = (turning left, keeping straight, turning right) to the input $I^{(t)}$. The IIM uses the classification cross entropy loss as the loss function. We use Adam optimizer, and define the learning rate $\alpha = 0.0005$ and decay rate $\sigma = 0.9$.

2.2 Dataset selection and description

In this paper, we select US-101 section and I-80 section of next generation simulation (NGSIM) [28] dataset for training and testing. NGSIM dataset consists of 11779 real highway traffic trajectories, recording the detailed parameters such as vehicle ID, lane ID, global ID, the frame time, speed, acceleration, and time headway, and is useful for intention identification and motion prediction. We divide the dataset into training set and test set and set the sampling frequency of the experimental data as 5 Hz to reduce the operation cost. Meanwhile, we also filter the original data owing to the errors and noise disturbance.

For the IIM, we divide the extracted trajectory segments into three categories: turning left, keeping straight, and turning right, with corresponding marks attached. Referring to [25], the classification basis we employed in this paper follows the defined rule. The segment between the lane change start point and the lane change endpoint is defined as the lane change process, as shown in Figure 4.

We select the three types of scenarios (turning left, keeping straight, turning right) from the dataset. Because straight driving is a much more common scenario than lane changing, the keeping straight category has far more instances in the extracted sequences. Therefore, 5000 sequences (of a total 15000 sequences) are randomly selected from each of the three categories as the entire dataset, 80% of which belong to the training set and 20% belong to the test set in consistence with most typical experiments. All the extracted data need to be standardized to facilitate neural network training.
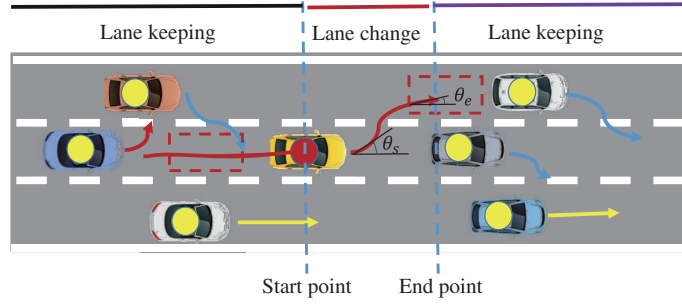
Figure 4 (Color online) Procedure of lane change. Three processes are defined in this figure according to the surrounding vehicle information and the trajectory of the predicted vehicle, where θ_s and θ_e are the heading angle threshold of the lane change start and end points, respectively.
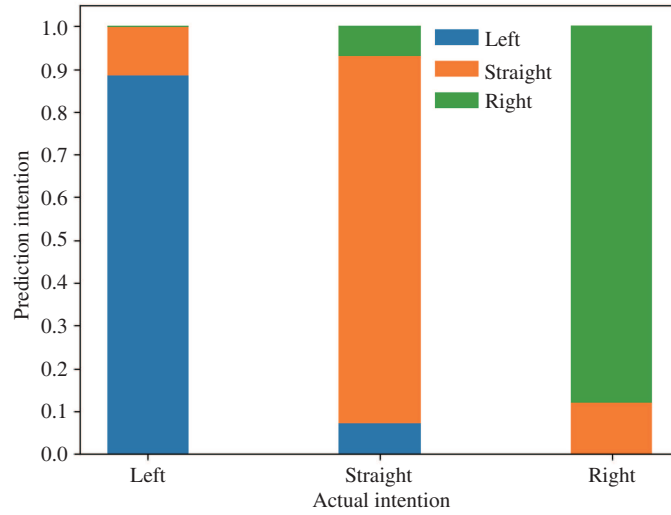

Figure 5 (Color online) The confusion matrix of intention identification. When the actual intention is keeping straight, the identification result turns to be the worst compared with recognizing the intention of turning left or turning right for two potential lanes, which will disturb the recognition process.

Table 1 Performance evaluation of different methods

Intention	Precision		Recall		Accuracy	
	IIM	SVM	IIM	SVM	IIM	SVM
Turning left	0.925	0.903	0.884	0.833		
Keeping straight	0.785	0.716	0.859	0.828	0.874	0.832
Turning right	0.927	0.907	0.880	0.835		

2.3 Performance analysis

The performance of the IIM directly affects the quality of trajectory prediction. We take SVM as the baseline to test the performance of the proposed IIM. Meanwhile, we employ the general evaluation indexes such as accuracy, precision, and recall for performance evaluation.

Because the IIM outputs the probabilities of three categories (turning left, keeping straight, turning right) and the corresponding mark has only one correct category, the category with the largest output probability is defined as the prediction category. The IIM is tested with the data in the test set. The confusion matrix of intention identification results is shown in Figure 5, and its performance evaluation compared with SVM is shown in Table 1.

From Figure 5, we can see the results of the confusion matrix of intention identification are relatively accurate. The predicted intention is consistent with real intention in all the three types of scenarios. From Table 1, we can see that the indicators of IIM proposed in this paper are all better than the traditional

SVM classifier. The recall rate and the overall accuracy rate of IIM for the three categories are all above 85%, which shows that the IIM has a good intention identification capability. The recognition accuracy rates of turning left and turning right are close to 92%, which is higher than the recognition accuracy rate of keeping straight. The reason may be that a small part of the original data have large chattering owing to some certain errors and noises, which makes the IIM easily misjudge these chattering data as a lane-changing behaviour. Furthermore, if a trajectory of any lane change category (right/left) is misjudged, it is seldom recognized as a category of the opposite (left/right) lane change direction, but easily recognized as the category of keeping straight, which also results in a lower accuracy rate of keeping straight category. Meanwhile, the information received by the IIM includes the state information of the predicted vehicle and the surrounding vehicles, which can support the predicted vehicle to make reasonable predictions.

3 Risk assessment considering intention identification

In this section, based on intention identification, an RAM considering the coupling mechanism of drivers, vehicles and roads is constructed. We analyze the interaction between road users quantitatively, and describe the influence degree of various traffic elements on driving risks. Based on the IIM and RAM, the driving risk can be quantified as a time-varying risk field continuously distributed in the traffic environment.

3.1 RAM based on driving safety field

The traffic environment includes not only ego vehicles but also other static and dynamic traffic participants. Owing to the inconsistency of movement states among traffic participants, the state of each traffic participant will change along with other road users. When the driving state of a certain traffic participant is significantly different from others in the traffic flow, traffic disturbance will occur and bring the potential risk [29, 30].

Under normal circumstances, driving risks usually occur between different traffic participants or between a road user and its surrounding environment. Driving risks cannot exist independently; therefore, to evaluate the risk level of the traffic environment, we adopt the risk field and define driving risk as the interaction of potential fields among various traffic participants in the traffic environment. Referring to the previous researches [31, 32], by analyzing the relationship between force and energy transformation in the collision process, we propose the theory of the equivalent force [32]. If traffic participant j drives freely at a constant velocity in the traffic environment and is considered as a particle, the traffic risk caused by the vehicle in the environment meets the isotropy on the plane because traffic participant j can drive in any direction. Therefore, the field force $F_{ji,0}$ can be defined as

$$
F_{ji} = \begin{cases} E_{j,0}, & r_{ji} \in [0, r_{\min}), \\ E_{j,0} r_0 \left(\dfrac{1}{r_{ji}^2} - \dfrac{1}{r_{\max}^2} \right), & r_{ji} \in [r_{\min}, r_{\max}], \\ 0, & r_{ji} \in (r_{\max}, +\infty), \end{cases} \tag{5}
$$

where we define $r_{ji}^2 = x_{ji}^2 + y_{ji}^2$, and according to the specific constraints, we define the relationship between $r_{\min}$ and $r_{\max}$ as $r_{\min} = r_{\max} \sqrt{\frac{r_0}{r_{\max}^2 + r_0}}$.

Furthermore, $E_{j,0}$ represents the kinetic energy, when $r_{ji} \in [0, r_{\min})$; $F_{ji,0}$ is numerically equal to $E_{j,0}$; r_0 is the radius of the driver's focus, which is related to the distance between the driver and the vehicle; x_{ji} and y_{ji} represent the distance of traffic participant j from any point i in the longitudinal direction and the lateral direction respectively; $r_{\max}$ is the distance between free-flowing vehicles and can represent the maximum impact range of risk. It is defined according to the traffic manual. Because $F_{ji,0}$ takes constant value range when $r_{ji} \in [0, r_{\min}) \cup (r_{\max}, +\infty)$, it is associated with the change of r_{ji} only when $r_{ji} \in [r_{\min}, r_{\max}]$. As a result, the subsequent study mainly focuses on $r_{ji} \in [r_{\min}, r_{\max}]$. Therefore, the

gradient change of the driving safety field force $F_{ji,0}$ generated during the movement of the vehicle is defined as follows:

$$\nabla F_{ji,0} = -\frac{2E_{j,0}r_0}{\left(x_{ji}^2 + y_{ji}^2\right)^2} \cdot \left(x_{ji} \cdot i + y_{ji} \cdot j\right). \tag{6}$$

Meanwhile, in real traffic environment, drivers need to be subjected to the constraints of traffic rules in the driving process, and they will not be subject to the driving risks caused by isotropic directional movements to the outside world. Under normal circumstances, from the perspective of driver's subjective feelings or objective collision probability, the risks to traffic environment in the positive direction are greater than the negative direction in the driving process, which is similar to the Doppler shift effect of waves [33]. In the Doppler shift effect, the movement of the wave source leads to an increase in the frequency received by the observer on one side of the movement direction and a decrease in the frequency received by the observer on the negative direction:

$$f_s' = \frac{v_{s,0} \pm v_o(t)}{v_{s,0} \mp v_s(t)} f_s, \tag{7}$$

where f_s' is the frequency at the location of the observer; f_s is the initial frequency of the wave source; $v_{s,0}$ is wave velocity); $v_o(t)$ is the observer's velocity (we set the direction closed to the wave source as positive, while away from the wave source as negative); $v_s(t)$ is the velocity of the wave source; and the direction is defined as negative towards the observer while positive away from the observer.

According to the existed research, drivers mainly rely on vision to obtain information in the driving process [34], and they are sensitive to the relative distance and relative speed between other road users and themselves. Therefore, from the perspective of the driver, the risk that vehicle i is exposed to vehicle j in the traffic environment can be described by the driving safety field as follows:

$$F_{ji,0} = E_{j,0} \left(\frac{r_0}{k_{x,0}x_{ji}^2 + k_{y,0}y_{ji}^2} - \frac{1}{r_{\max}} \right), \tag{8}$$

$$E_{j,p} = \frac{1}{2}m_j \left(v_j - v_i\right)^2, \tag{9}$$

where $k_{x,0}$ and $k_{y,0}$ are the longitudinal and lateral gradient adjustment coefficients respectively; m_j represents the mass of vehicle j.

3.2 Determination of influence range of driving risk

Traffic marking is significant in restricting driving risks by constraining drivers' behaviors. They can make the risks caused by road users to the traffic environment vary in both lateral and longitudinal directions. Besides, drivers' perception of the environment is closely related to their visual characteristics. The visual recognition ability of driver's naked eye is greatly affected in the driving process. With the increase of vehicle speed, the field of view becomes narrower. Researchers regard the driver's field of view as an ellipse [35]. Therefore, the risks to the traffic environment caused by vehicles in the longitudinal and lateral directions have a significant difference during the driving process.

According to the analysis of the driver's normal driving behavior, the risk distribution generated by road users in traffic environment is represented by an ellipse as shown in Figure 6. A_1A_2 and B_1B_2 are the major axis and the minor axis of the ellipse respectively, and their relationship can be defined as $A_1A_2 = 2A_1j = 2jA_2 = 2A_j$, $B_1B_2 = 2B_1j = 2jB_2 = 2B_j$. Meanwhile, the ellipse shown in Figure 3 is a contour line of the risk field caused by vehicle j in the environment.

Considering that a driver always abides by the rules and ensures safe driving as much as possible, then he will maintain a certain headway in the driving process. Besides, the traffic rules stipulate that drivers are not allowed to change lanes continuously. Furthermore, dynamic disturbances while ensuring the control stability of intelligent vehicles should be considered to deal with dynamic uncertainties of risk
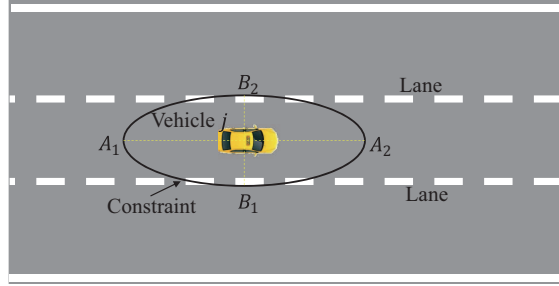
Figure 6 (Color online) Elliptic constraint effect of road marking on traffic risk. The two dotted lines have the function of constraining vehicle j to follow the centerline of its own lane, and hence when vehicle j keeps straight, the influence range will turn to be in its own lane without any intention to change lane.

assessment [36]. Combining with the geometric dimensions of the vehicle, the lengths of the semi-major axis and semi-minor axis of the ellipse in Figure 6 are set as follows:

$$A_j = r_0 + l_1, \quad B_j = l_w + l_2, \tag{10}$$

where A_j is the semi-long axis of the ellipse; l_1 is half the length of the vehicle; B_j is an oval semi-minor axis; l_w denotes the lane width (here we define $l_w = 3.5$ m); and l_2 is half the width of the vehicle. Note that the major axis of the ellipse is a function related to the vehicle velocity; hence the smaller the velocity; the smaller the major axis. Therefore, to avoid the length of the major axis being smaller than that of the minor axis, we set $r_0 \geqslant l_w$. Affecting by the lateral restraint of lane lines, there are obvious differences in risk distribution in lateral and longitudinal directions when driving. The essence of the ellipse shown in Figure 6 is the dynamic influence range after considering the effect factors from the longitudinal and lateral direction; for example, the longitudinal direction can be affected by the safety time interval, traffic flow speed, etc., while the lateral direction can be influenced by lane constraints. Hence, the risk caused by vehicle j is distributed according to the black contour lines as follows:

$$k_{x,d} x_{ji}^2 + k_{y,d} y_{ji}^2 = r_{ji'}^2, \tag{11}$$

where $k_{x,d}$ and $k_{y,d}$ are the gradient adjustment coefficient in the longitudinal direction and the lateral direction respectively. According to the elliptical characteristics shown in Figure 6, we can obtain

$$k_{x,d} = 1, \quad k_{y,d} = \frac{A_j^2}{B_j^2}, \tag{12}$$

where A_j and B_j are respectively the semi-major axis length and the semi-minor axis length of the ellipse. According to the geometric characteristics of the ellipse, we can calculate the relationship:

$$x_{ji} = \frac{r_{ji'}}{\sqrt{k_{x,d}}} \cos t, \quad y_{ji} = \frac{r_{ji'}}{\sqrt{k_{y,d}}} \sin t, \tag{13}$$

where $t \in [0, 2\pi]$. The distance from the center of the vehicle j to a point i on the ellipse is

$$r_{ji} = \frac{r_{ji'} \cos t}{\sqrt{k_{x,d}} \cos \theta_{ji}}, \tag{14}$$

where θ_{ji} is the included angle between the line connecting the vehicle j and the point i and the velocity direction of the vehicle j. Then,

$$\frac{k_{x,d}}{k_{y,d}} \sin^2 \theta_{ji} + \cos^2 \theta_{ji} = \frac{\cos^2 \theta_{ji}}{\cos^2 t}. \tag{15}$$

Finally, the dynamic influence range of field force can be described as an ellipse, in which r_{ji} can be calculated as

$$r_{ji} = \frac{r_{ji'}}{\sqrt{k_{x,d} \cos^2 \theta_{ji} + k_{y,d} \sin^2 \theta_{ji}}}. \tag{16}$$
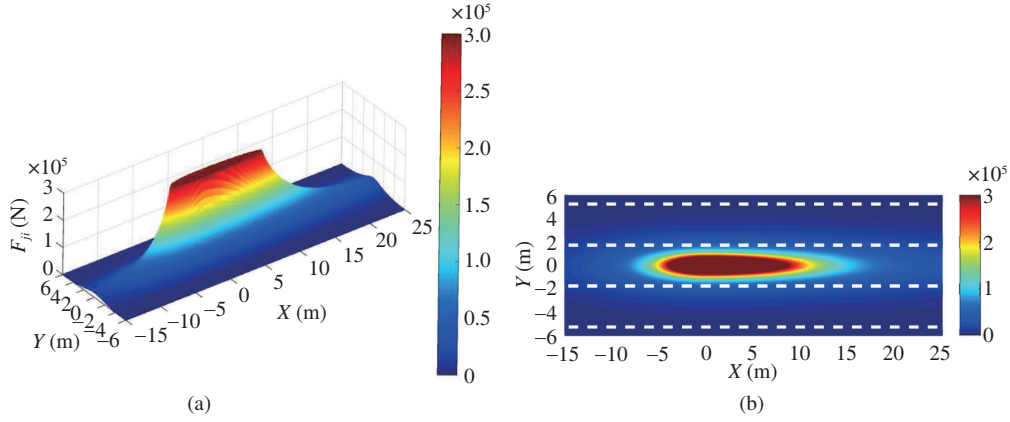
Figure 7 (Color online) Force distribution of driving safety field under traffic marking restriction.

3.3 Comprehensive risk evaluation model based on IIM and RAM

The occurrence of traffic accidents can be understood as abnormal energy transfer. Therefore, based on the kinetic energy of the vehicle in the driving process, we analyze the direct risk caused by road users in traffic environment and the disturbance risk caused by traffic flow. Besides, we discover the relationship between the potential risk and the various attributes of traffic participants in environment, such as types of road users, the establishment of road traffic facilities, and the influence of driver's behaviors. Finally, we establish a comprehensive driving risk evaluation model reflecting the interaction between drivers, vehicles, and the road. Based on this model, the risks caused by vehicles to traffic environment can be expressed by

$$F_{ji,0} = E_{j,0} r_0 \left[\frac{1}{r_{ji}^2 (k_{x,d} \cos^2 \theta_{ji} + k_{y,d} \sin^2 \theta_{ji})} - \frac{1}{r_{\max}^2} \right]. \tag{17}$$

Turn the above function to a rectangular coordinate system:

$$F_{ji,0} = E_{j,0} r_0 \left(\frac{1}{k_{x,d} x_{ji}^2 + k_{y,d} y_{ji}^2} - \frac{1}{r_{\max}^2} \right). \tag{18}$$

Therefore, if the driver strictly abides by the traffic rules, the field generated by vehicle j in traffic environment is shown in Figure 7. Under the restriction of road traffic marking, the vertical and horizontal risk distributions are obviously different.

When considering the behavioral requirements of traffic participants, risk assessment can assess better future behavior. Therefore, with the help of the intention identification factors based on IIM, we propose a comprehensive risk evaluation model that is continuous in time, and introduce a predictive risk map based on the possible dynamic changes of these traffic participants. The predictive risk map that presents the possibility of one certain action shows the importance of behavior identification in the future. Hence, we use the predictive risk map for future behavior assessment and planning shown in Figure 8, and the sum of the distribution of predicated risk force $F_{ki,m}$ in each intention direction is equal to the total predicated risk force F_{ki}. Specifically, $F_{ki,m}$ is obtained by multiplying the field force $F_{ji,0}$ by the intention identification factor p_m in each direction. The relational expression is as follows:

$$F_{ki} = \sum_{m=1}^{3} F_{ki,m} = \sum_{m=1}^{3} p_m F_{ji,0}. \tag{19}$$

4 Experiment and result analysis

In this section, we conducted both simulation experiments and naturalistic driving experiments to verify the effectiveness of the proposed model in typical but challenging scenarios. Accidents often happen
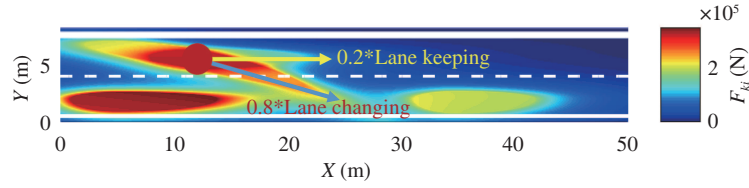
Figure 8 (Color online) The predictive driving risk map. Combining IIM and RAM, a predictive risk map with intention possibility can describe the influence range and trend. In this example, we output the predicted vehicle with a 20% lane-keeping probability ($p_3 = 0.2$) and an 80% lane-changing probability ($p_1 = 0.8, p_2 = 0$) predicted by the IIM. Therefore, the distribution and magnitude of the field force are also proportional to 20% and 80% in the straight-line direction and the lane change direction.
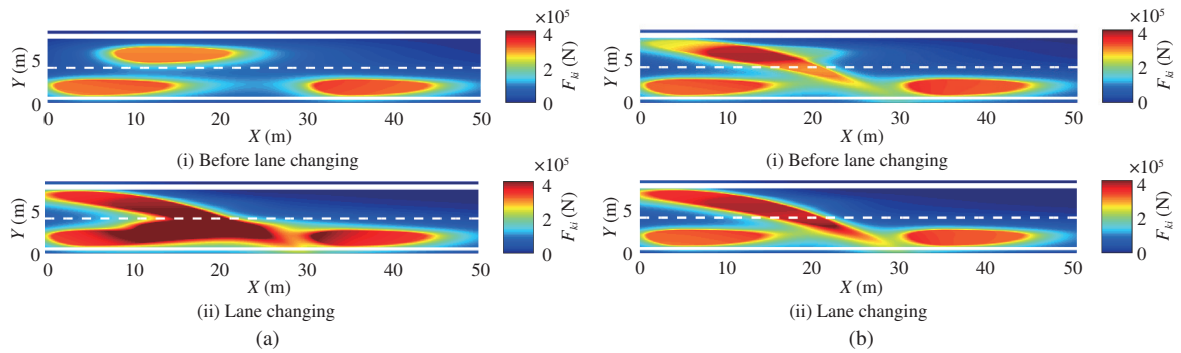

Figure 9 (Color online) Two different examples of driving risk maps. If there is no behavior prediction, it is assumed that all vehicles in the traffic map are stable and do not change their states suddenly. As time goes by, the behaviors of surrounding vehicles will change suddenly, resulting in possible collision risks when there is no early warning. Introducing the intention identification will ensure the reliability of planning and control in the subsequence stage. (a) An example of 'Perception-Assessment-Planning' architecture; (b) an example of 'Perception-Prediction-Assessment-Planning' architecture.

suddenly when cut-in behaviors disturb normal driving. Therefore, we first design simulation experiments to test the performance of the proposed model in cut-in scenario. Then, naturalistic data analysis using the highD Dataset [37] is employed to present the potential application of the proposed model.

4.1 Simulation experiment: performance comparison of different architectures

We use MATLAB application driving scenario designer to design these driving scenarios. The vehicle in the lower left of each subgraph of Figure 9 is the host vehicle, which has the perception ability by equipping with radars and front cameras. Hence, the intelligent vehicle can detect the surrounding environment, assess the dynamic state and plan its specific route to the destination. The two simulation scenarios in Figure 9 present two different architectures of the autonomous system. Figure 9(a) shows the 'Perception-Assessment-Planning' architecture, without intention identification, and these three vehicles are driving normally before the upper left vehicle cuts in. While sudden cut-in behavior happens, it turns to be dangerous as shown in (ii). Three vehicles in the traffic map are affected by unexpected disturbance, particularly, there is a collision risk owing to the lack of early warning of the cut-in vehicle and the rear vehicle in the right lane.

Figure 9(b) states the 'Perception-Prediction-Assessment-Planning' architecture, and the algorithm of the specific comprehensive risk evaluation model is shown in Algorithm 1. Firstly, the host vehicle detects the states of surrounding vehicles and predicts the maneuver intention using the IIM. In Figure 9(b), (i) describes that before lane changing, the host vehicle can predict the cut-in intention of the upper left vehicle. Then, we define the threshold force of the warning F_{th} to assistant intelligent vehicle. A dynamic and real-time risk assessment of mixed traffic allows the host vehicle to get an early warning. Finally, more reliable planning of maneuvers can be achieved in the subsequent process. (ii) shows that in the cut-in process, with the help of advanced prediction, the host vehicle can get an early warning and slow down before the predicted cut-in behavior. Results shown in the two maps demonstrate the significance

---

Algorithm 1 Risk assessment based on IIM and RAM

1: Initialize $m_j, r_{\max}, v_j, \theta_{ji}, k_{x,d}, k_{y,d}, A_1 A_2, B_1 B_2, r_0$;

2: Get the initial state of the predicted vehicle $V_e^{(t)}$ and surrounding vehicles $V_{hi}^{(t)}$;

3: Set up the IIM;

4: **for** $i = 1$ to n (traffic participants) **do**

5:     Input the interaction state: $I^{(t)} = [V_h^{(t)}, S^{(t)}], t = (T - T_p, \ldots, T - 1, T)$;

6:     Calculate the intention probability by using the Softmax function;

7:     Output the probability of the IIM: $p_m = P(l_m|I), \Omega = (p_1, p_2, p_3)$;

8: **end for**

9: **for** $m = 1$ to 3 **do**

10:     Define the driving risk force: $F_{ji,0} = E_{j,0}(\frac{r_0}{k_{x,0}x_{ji}^2 + k_{y,0}y_{ji}^2} - \frac{1}{r_{\max}})$;

11:     Define the risk range: $r_{ji} = \frac{r'_{ji}}{\sqrt{k_{x,d}\cos^2\theta_{ji} + k_{y,d}\sin^2\theta_{ji}}}$;

12:     Calculate the predictive driving risk force in this direction $F_{ki,m} = p_m F_{ji,0}$;

13:     Output the predictive risk map in this direction;

14: **end for**

15: Calculate the total predictive driving risk force: $F_{ki} = \sum_{m=1}^{3} F_{ki,m}$;

16: Output the total predictive risk map;

17: Define the threshold force F_{th} of active assistance based on the existed algorithm [19];

18: **if** $F_{ki} > F_{\text{th}}$ **then**

19:     Output("Danger from the surrounding vehicle" warning to vehicle j);

20: **else**

21:     Output("Safe driving" feedback to vehicle j);

22: **end if**

---

of the comprehensive risk evaluation model.

4.2 Naturalistic driving experiment: application of the comprehensive risk evaluation model

Based on IIM and RAM, we further analyze the performance of the proposed risk evaluation model in different scenarios. By extracting the lane-keeping and lane-changing scenarios respectively, we test the model via naturalistic driving dataset, output the dynamic risk values, and compare the predicted behavior with the actual manipulation behavior in real traffic scene. The real traffic dataset adopts the traffic flow data of the highD Dataset, which has a high resolution on the driving trajectory. And the dataset can directly extract the required scene through the video and visually display the historical trajectory and ID information of vehicles in a traffic map. Meanwhile, the analysis of a large number of naturalistic driving data is more consistent with the driver behavior, which can test the intelligence and anthropomorphism of the proposed model.

Subsection 4.1 has demonstrated the principle that a normal driver will pre-judge the behavior of surrounding participants and then assess the driving risk considering the vehicle-environment interaction. Basically, drivers will pursue efficiency on the premise of ensuring their own safety. For example, if there is a slow obstacle in his lane, he will choose to change the lane to achieve efficiency on the premise of safety. Otherwise, he will keep the original lane and keep a long distance from the obstacle. While from Figure 10, scenario 1 describes the lane-keeping behavior. The probability of the driver choosing to turn right is 0.92, and the probability of lane maintenance is 0.08. Therefore, the intention identification factor is input into the RAM to obtain the risk distribution in the traffic scene, as shown in Figure 11(a). Scenario 1 reflects the risk assessment of different vehicles in traffic map from the perspective of traffic. The result of intention identification of ID371 is shown in the histogram on the left side of Figure 10. It can be seen that ID371 will keep straight along the lane with a high probability, so the two figures before and after the prediction can reflect the consistency with dynamic risk intensity and trend after it keeps straight in real traffic.

The result of intention identification for ID97 is shown in the second histogram on the left in Figure 10. In scenario 2, the probability of the intelligent vehicle choosing to turn right is 0.84 and the probability of lane maintenance is 0.16. Similarly, the intention identification factor is input into the RAM to obtain the risk distribution in the traffic scene, as shown in Figure 11(b). The deeper the color in the map, the higher
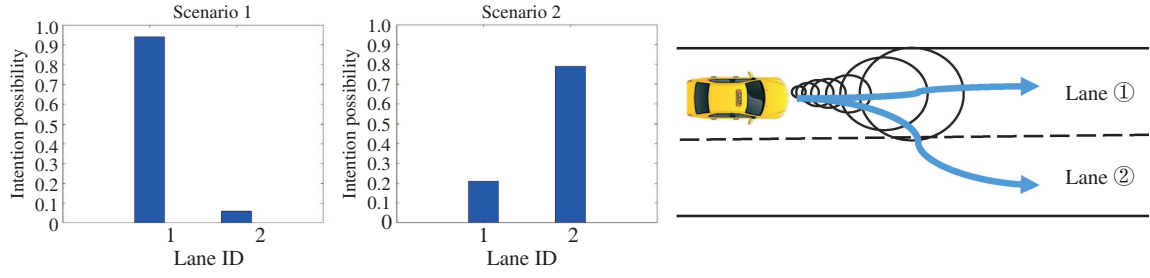
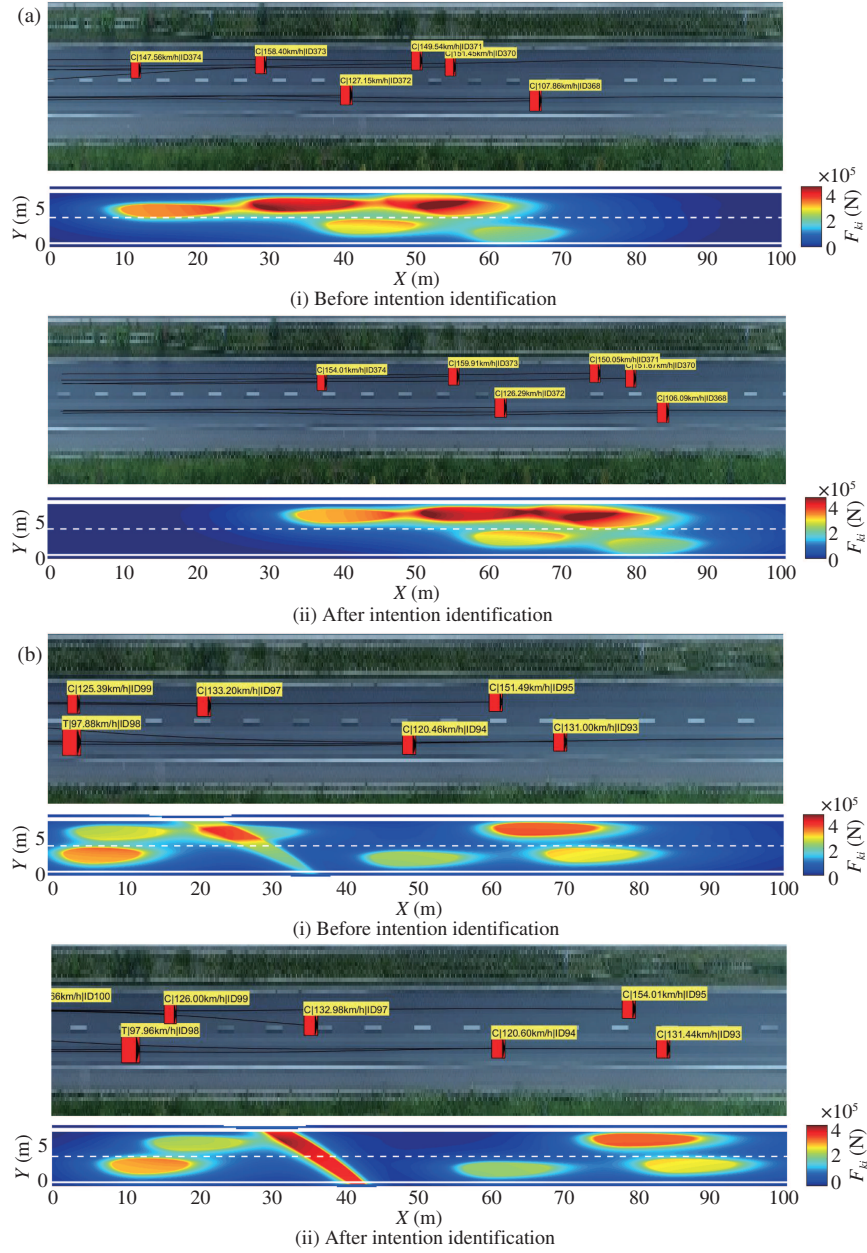**Figure 10** (Color online) Trajectory prediction of a surrounding vehicle.

Figure 11 (Color online) Traffic risk maps of naturalistic driving scenarios. The top picture of each subgraph is the real scenario extracted from the highD Dataset. The red block in the figure represents the moving vehicle, the yellow label indicates the speed and ID of each vehicle, and the color depth in the map represents the risk intensity affected by the vehicle's speed, quality, and relative position with surrounding vehicles. (a) Naturalistic lane-keeping scenario; (b) naturalistic cut-in scenario.

the risk intensity. In (i), the intelligent vehicle has perceived the intention of lane-changing in advance, showing a trend of risk distribution bifurcating. Meanwhile, in the cut-in process, the host vehicle (ID98) that is cut in by other vehicles, has got the corresponding information, so the cut-in behavior does not disturb its driving state. Meanwhile, as shown in (ii), the risk impact range of the cut-in vehicle (ID97) is constrained by the outermost lane line, restricting the risk impact range within the lane.

Through the analysis of the above results, it can be seen that the integrated risk evaluation model can accurately quantify the risks of the host vehicle and surrounding vehicles, and provide sufficient time for these intelligent vehicles to respond to various complex dangerous situations by considering the uncertainty of risks and giving an early warning. In future work, we will be able to output the critical point based on the current driving risk, and to ensure that the decision-making process of autonomous vehicle is always within the scope of safety threshold. By developing risk-bounded decision-making algorithm, intelligent vehicles can be supported to deal with dangerous driving situations and realize reliable driving.

5 Conclusion and future work

This paper presents a probabilistic risk assessment framework for quantitative analysis of driving risk with uncertainty estimation. The integrated framework enables intelligent vehicles to perceive and assess the dynamic driving risk accurately, and provides a predictive risk map to deal with uncertainties caused by the immediate behavior changes of surrounding traffic. The novelty of this contribution is that it extends the influence range in advance and improves safety level for the high dimensional risk assessment. This distinguishes with existing algorithms tackling the similar challenges.

Potential appealing properties include that the whole model can gain a better understanding of the factors that affect the probability of hazardous accidents, and provide a method for better predicting and reducing the likelihood of incidents for intelligent vehicles. Future work will focus on the application of the proposed model for the decision-making of intelligent vehicles, such as extracting critical points to avoid accidents and setting safety threshold to keep driving within a safe range.

References

1 González D, Pérez J, Lattarulo R, et al. Continuous curvature planning with obstacle avoidance capabilities in urban scenarios. In: Proceedings of 17th International IEEE Conference on Intelligent Transportation Systems (ITSC14), 2014. 1430–1435
2 González D, Pérez J, Milanes V, et al. A review of motion planning techniques for automated vehicles. IEEE Trans Intell Transp Syst, 2016, 17: 1135–1145
3 Tas O S, Kuhnt F, Zollner J M, et al. Functional system architectures towards fully automated driving. In: Proceedings of 2016 IEEE Intelligent Vehicles Symposium (IV), Gotenburg, 2017. 304–309
4 Mayfield H J, Smith C S, Lowry J H, et al. Predictive risk mapping of an environmentally-driven infectious disease using spatial Bayesian networks: a case study of leptospirosis in Fiji. PLoS Negl Trop Dis, 2018, 12: e0006857
5 Guo H, Shen C, Zhang H, et al. Simultaneous trajectory planning and tracking using an MPC method for cyber-physical systems: a case study of obstacle avoidance for an intelligent vehicle. IEEE Trans Ind Inf, 2018, 14: 4273–4283
6 Wu C, Peng L, Huang Z, et al. A method of vehicle motion prediction and collision risk assessment with a simulated vehicular cyber physical system. Transpation Res Part C-Emerg Technol, 2014, 47: 179–191
7 Kim J, Kum D. Collision risk assessment algorithm via lane-based probabilistic motion prediction of surrounding vehicles. IEEE Trans Intell Transp Syst, 2018, 19: 2965–2976
8 Katrakazas C, Quddus M, Chen W H, et al. Real-time motion planning methods for autonomous on-road driving: state-of-the-art and future research directions. Transpation Res Part C-Emerg Technol, 2015, 60: 416–442
9 Lee K Q, Peng H. Evaluation of automotive forward collision warning and collision avoidance algorithms. Vehicle Syst Dyn, 2005, 43: 735–751
10 van Winsum W. The human element in car following models. Transpation Res Part F-Traffic Psychol Behaviour, 1999, 2: 207–211

11 Li Y, Zheng Y, Wang J Q, et al. Crash probability estimation via quantifying driver hazard perception. Accident Anal Prevention, 2018, 116: 116–125

12 Archibald J K, Hill J C, Jepsen N A, et al. A satisficing approach to aircraft conflict resolution. IEEE Trans Syst Man Cybern C, 2008, 38: 510–521

13 Minderhoud M M, Bovy P H L. Extended time-to-collision measures for road traffic safety assessment. Accident Anal Prevention, 2001, 33: 89–97

14 Allen C, Ewing M, Keshmiri S, et al. Multichannel sense-and-avoid radar for small UAVs. In: Proceedings of IEEE/AIAA 32nd Digital Avionics Systems Conference (DASC), 2013

15 Khatib O. Real-time obstacle avoidance for manipulators and mobile robots. In: Proceedings of IEEE International Conference on Robotics and Automation, 1985. 500–505

16 Reichardt D, Shick J. Collision avoidance in dynamic environments applied to autonomous vehicle guidance on the motorway. In: Proceedings of the Intelligent Vehicles'94 Symposium, Paris, 1994. 74–78

17 Huang Y, Ding H, Zhang Y, et al. A motion planning and tracking framework for autonomous vehicles based on artificial potential field elaborated resistance network approach. IEEE Trans Ind Electron, 2020, 67: 1376–1386

18 Hu X, Chen L, Tang B, et al. Dynamic path planning for autonomous driving on various roads with avoidance of static and moving obstacles. Mech Syst Signal Process, 2018, 100: 482–500

19 Wang J Q, Wu J, Zheng X J, et al. Driving safety field theory modeling and its application in pre-collision warning system. Transpation Res Part C-Emerg Technol, 2016, 72: 306–324

20 Aoude G S, Luders B D, Lee K H, et al. Threat assessment design for driver assistance system at intersections. In: Proceedings of the 13th International IEEE Conference on Intelligent Transportation Systems, 2010. 1855–1862

21 Goerlandt F, Reniers G. On the assessment of uncertainty in risk diagrams. Saf Sci, 2016, 84: 67–77

22 Xie G T, Zhang X, Gao H B, et al. Situational assessments based on uncertainty-risk awareness in complex traffic scenarios. Sustainability, 2017, 9: 1582

23 Belkhouche F. Modeling and calculating the collision risk for air vehicles. IEEE Trans Veh Technol, 2013, 62: 2031–2041

24 Havlak F, Campbell M. Discrete and continuous, probabilistic anticipation for autonomous robots in urban environments. 2013. ArXiv: 1309.0766

25 Deo N, Trivedi M M. Multi-modal trajectory prediction of surrounding vehicles with maneuver based LSTMs. In: Proceedings of IEEE Intelligent Vehicles Symposium (IV), 2018. 1179–1184

26 Khosroshahi A, Ohn-Bar E, Trivedi M M. Surround vehicles trajectory analysis with recurrent neural networks. In: Proceedings of IEEE 19th International Conference on Intelligent Transportation Systems (ITSC), Rio de Janeiro, 2016. 2267–2272

27 Tijerina L, Garrott W R, Stoltzfus D, et al. Eye glance behavior of van and passenger car drivers during lane change decision phase. Trans Res Rec, 2005, 1937: 37–43

28 Federal Highway Administration. Next Generation Simulation (NGSIM) Program. 2006. http://ngsim-community.org/

29 Yoshitake H, Shino M. Risk assessment based on driving behavior for preventing collisions with pedestrians when making across-traffic turns at intersections. IATSS Res, 2018, 42: 240–247

30 Zou Y, Qu X B. On the impact of connected automated vehicles in freeway work zones: a cooperative cellular automata model based approach. J Intell Connected Veh, 2018, 1: 1–14

31 Zheng X J, Huang H Y, Wang J Q, et al. Behavioral decision-making model of the intelligent vehicle based on driving risk assessment. Comput-Aided Civil Infrastruct Eng, 2019, 16: 1–18

32 Zheng X J, Huang B, Ni D H, et al. A novel intelligent vehicle risk assessment method combined with multi-sensor fusion in dense traffic environment. J Intell Connected Veh, 2018, 1: 41–54

33 Seddon N, Bearpark T. Observation of the inverse Doppler effect. Science, 2003, 302: 1537–1540

34 Zhang W, Dai J, Pei Y, et al. Drivers' visual search patterns during overtaking maneuvers on freeway. Int J Environ Res Public Health, 2016, 13: 1159

35 Chen T, Wen H, Hu H, et al. On-orbit assembly of a team of flexible spacecraft using potential field based method. Acta Astronaut, 2017, 133: 221–232

36 Guo H, Liu J, Dai Q, et al. A distributed adaptive triple-step nonlinear control for a connected automated vehicle platoon with dynamic uncertainty. IEEE Internet Things J, 2020, 7: 3861–3871

37 Krajewski R, Bock J, Kloeker L, et al. The highD Dataset: a drone dataset of naturalistic vehicle trajectories on German highways for validation of highly automated driving systems. 2018. ArXiv: 1810.05642